Colloids and Surfaces A: Physicochem. Eng. Aspects 432 (2013) 71–81

Contents lists available at SciVerse ScienceDirect

Colloids and Surfaces A: Physicochemical and Engineering Aspects

journal homepage: www.elsevier.com/locate/colsurfa

Wetting dynamics and evaporation of sessile droplets on nano-porous alumina surfaces

Sanchit K. Singh [a], Sameer Khandekar [a,*], Dheeraj Pratap [b], S. Anantha Ramakrishna [b]

[a] Department of Mechanical Engineering, Indian Institute of Technology Kanpur, India
[b] Department of Physics, Indian Institute of Technology Kanpur, India

HIGHLIGHTS

- Spreading dynamics of water droplets on nano-porous alumina surface.
- 3D-Laser Confocal Microscopy of equilibrium and wetting transition of droplets.
- Bulk evaporation rates of sessile droplets on nano-textured alumina surfaces.
- Effect of nano-pore distribution on equilibrium, spreading and evaporation rates.

GRAPHICAL ABSTRACT

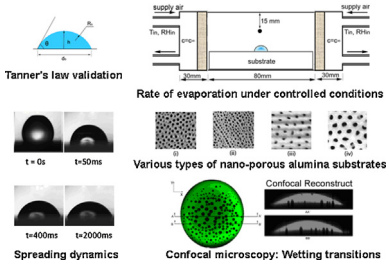

ARTICLE INFO

Article history:
Received 15 March 2013
Received in revised form 29 April 2013
Accepted 30 April 2013
Available online 14 May 2013

Keywords:
Droplet evaporation
Diffusion
Nanostructured surfaces
Droplet spreading
Wetting transitions
Laser Confocal Microscopy

ABSTRACT

An experimental investigation of wetting and evaporation of sessile droplets is presented on nano-porous alumina substrates having different pore distribution (uniform, random and linearly arranged) morphologies and pore sizes (70–120 nm). Firstly, the behavior of a droplet as it spreads and wets a surface is captured using high speed videography and benchmarked with the correlation given by the Tanner's law. The Cassie–Wenzel state transition of a droplet on nano-porous surfaces is also scrutinized with 3D-Laser Confocal Microscopy which clearly reveals the sub-stages of the transition process. During wetting transition, entrapped air bubbles are seen coming out of the nano-porous substrate, which lead to micro-convection. In this study, sessile droplet evaporation on the nano-textured surfaces is also investigated. Evaporation can be considered as a quasi-steady-state process, such that the vapor concentration distribution above the droplet satisfies the Laplace equation, but with a time-varying droplet surface. For benchmarking, the evaporation of sessile water and ethanol droplets on standard borosilicate glass and Teflon surfaces is examined, and results are compared with available diffusion models. Contact angle variation with time is recorded along with rate of evaporation in a controlled environment with specified humidity and temperature boundary condition. The coupling between wettability and eventual rate of droplet evaporation is established. The results clearly show that nano-structuring is an effective tool to control wettability as well as the diffusive evaporation process. In addition, the physical morphology and pore distribution affects wettability as well as evaporation rates.

1. Introduction

In recent years, due to the advent of nanotechnology, the deceptively simple problem of droplet spreading and evaporation is again attracting attention (Bonn et al. [1], Erbil [2]). Surface chemistry and energy distribution plays a key role in determination of wetting behavior, and much research has been devoted to obtain specific

* Corresponding author. Tel.: +91 512 259 7038; fax: +91 512 259 7408.
E-mail addresses: samkhan.iitk@gmail.com, samkhan@iitk.ac.in (S. Khandekar).

0927-7757/$ – see front matter © 2013 Elsevier B.V. All rights reserved.
http://dx.doi.org/10.1016/j.colsurfa.2013.04.070

Nomenclature

B	dimensionless constant
D	diffusion coefficient (m^2/s)
c	concentration of vapor (kg/m^3)
t	time (s)
m	mass of droplet (kg)
C	capacitance ($A^2\ s^4/kg^1\ m^2$)
C_x	ratio of C and $4\pi\varepsilon_o$ (m)
e	base of the natural logarithm = 2.71828
θ	contact angle of the droplet (°)
T	temperature (°C)
L	length/characteristic length (m)
R	radius of curvature of droplet (m)
R^*	non-dimensional radius
H^*	non-dimensional height
r	contact radius of droplet (m)
h	height of droplet (m)
g	acceleration due to gravity (m/s^2)
l_c	capillary length (m)

Greek symbols

μ	dynamic viscosity (kg/s m)
γ	surface tension (N/m)
ρ	mass density (kg/m^3)
ε_o	permittivity of free space ($kg\,m^3/A^2\ s^4$)

Non-dimensional numbers

Ca	capillary number ($\mu U/\gamma$)

Subscripts

o	initial
ap	apparent
eq	equilibrium
b	base of droplet
s	surface of sphere
c	capillary

wetting properties (Sun et al. [3,4]). Bonn et al. [1] has comprehensively compiled the developments in the field of wetting and spreading. Wetting plays a key role in many engineering fields. At large scales, it plays an important role in oil recovery, efficient deposition of pesticides on plant leaves, drainage of water from highways and on a smaller scale, in micro-fluidics, nano-printing, inkjet printing, etc. (Tabeling [5]). Droplet evaporation plays a vital role in various engineering fields, such as air/fuel-premixing, biological crystal growth and painting, to name a few. Similarly, evaporation of fuel droplets is well-known to have a strong influence on the pollutant emissions, ignition delays and overall combustor efficiency (Deprédurand et al. [6]). The equilibrium contact angle (which can be related to droplet height once volume and base contact radius is fixed) and vapor–air surface area play an important role in the rate of evaporation of the sessile drop (Rowan et al. [7]). Hence, the phenomenon of wettability on a substrate and rate of evaporation are strongly coupled in many applications.

From a fundamental as well as practical engineering viewpoint, three configurations of droplet evaporation are of interest: (i) evaporation of simple fluids on plain surfaces; (ii) evaporation of nanofluids (simple fluids containing suspended nano-particles) on plain surfaces; and (iii) evaporation of simple fluids on prefabricated micro/nano-structured surfaces. While the first case represents the classical problem of droplet evaporation, wherein decent amount of literature already exists, the latter two cases are not yet comprehensively explored. A theoretical study of first case, i.e. of simple fluids evaporating on plain surfaces, has been done analytically by Picknett and Bexon [8]. They distinguished two modes of evaporation: (i) at constant contact angle, with diminishing base contact area and; (ii) at constant base contact area with diminishing contact angle. Hu and Larson [9] numerically solved the Laplace equation to get vapor concentration distribution and the evaporation flux using finite element method. They used a microscopic particle tracer method to measure the rate of droplet evaporation in their experiments and compared the result to that derived by Picknett and Bexon [8] and results obtained from FEM analysis. The average relative discrepancy between the two predictions was observed to be less than 1%.

The case (ii) of evaporating drops containing colloidal particles on a solid substrate can be used for dispensing or organizing small particles suspended within them [10]. The dried deposit is not always uniform (e.g. coffee-ring pattern), and is caused by enhanced evaporation at the wetting line, as explained by Deegan et al. [11]. Chen et al. [12] studied the effect of addition of laponite, Fe_2O_3 and Ag nanoparticles in deionized water on evaporation rates and reported that these nanofluid droplets evaporate at different rates.

Evaporation of droplets of simple fluid on surfaces with nano-projection (case (iii)) was studied recently by Lee et al. [13] who reported that the surface structure is a more important factor than the initial contact angle when determining the characteristics of droplet evaporation. Choi and Kim [14] also investigated evaporation of sessile droplets of pure water and protein solution on Cu-based hydrophobic surfaces with nanoposts. The work done so far focuses on the evaporation dynamics on surfaces with nano-projections. However, evaporation on nanoporous surfaces is yet to be fully explored. Recently, Sobac and Brutin [15] studied the influence of the surface properties (roughness and the surface energy) on the evaporation process using various nano- and micro-coatings (PFC, PTFE, SiO_C, and SiO_x). They found that the evaporative rate is proportional to the dynamics of the wetting radius, i.e. the more a droplet wets and pins to a substrate, the shorter the evaporation time. In the subsequent study [16], they investigated the influence of the substrate temperature and thermal properties on the evaporation process. They used two nano-coatings (PFC and SiO_x), on various base substrates (copper, brass, bronze, and polyoxymethylene (POM)) to have widely different thermal conductivities. It was reported that the global evaporation rate appears clearly influenced by the thermal diffusivity of the substrate–the situation involves conjugate heat transfer. In addition, the contact angle evolution is modified with an increase in the substrate temperature.

In this paper, we focus our attention on evaporation of simple fluids on prefabricated micro/nano-structured surfaces [17]. The purpose of the present work is to study how nano-porous surfaces alter the wettability, spreading, equilibrium contact angle and rate of evaporation of sessile droplets of simple fluids, subjected to controlled thermal boundary conditions. In addition, nano-porous surfaces may lead to wetting transitions [18], the mechanism of which has been visualized in this work.

2. Theoretical background

2.1. Spreading of droplet

A droplet placed on a solid surface will, in general, be far from the equilibrium state and hence a flow is set in motion until the equilibrium apparent contact angle is attained. Tanner's law is observed when (i) a droplet is spreading on a wetting substrate, (ii) Laplace pressure is dominating in the bulk of the droplet, (iii) the fluid is viscous and nonvolatile, (iv) the small angle approximation for the contact angle is generally valid, and (v) the droplet

experiences a predominant interplay of surface tension and viscous forces, with negligible gravity and inertia forces. When these relatively restrictive constraints are not met, deviations from Tanner's law are observed [1,19].

If the radius of the droplet is less than the capillary length, $l_c = \sqrt{\gamma/(\rho g)}$, the droplet can be approximated by a spherical cap geometry. The speed of spreading is controlled by the balance of the available energy (surface or gravitational energy) and viscous dissipation, which mostly occurs near the contact line, but also in the bulk of the drop. A logarithmic plot of radius of a droplet spreading with time shows linear relation between the two, i.e. $r_b \propto t^n$, with value of $n = 1/10$ when the radius of the droplet is less than l_c (Tanner [20]). The spreading rate of the droplets, well described by the classical Tanner's law, given by:

$$r_b(t) \approx \left[\frac{10\gamma}{9B\mu}\left(\frac{4V_0}{\pi}\right)^3 t\right]^{1/10} \tag{1}$$

where V_0 is the droplet volume and γ is the liquid surface tension. This equation can be written as $r_b(t) \approx \alpha \cdot t^{110}$ where value of α can obtained from Eq. (1). B is a non-dimensional constant, the exact value is given by the following expression [1]:

$$B = \ln\left(\frac{r_b}{2e^2 L}\right) \tag{2}$$

where e is base of the natural logarithm and L is a characteristic length (set by microscopic effects like slip, long-ranged forces, or a diffuse interface).

In general, two drop equilibrium states are possible on a given rough surface (i) Cassie (the drop sits on top of the peaks of the rough surface) and (ii) Wenzel (liquid wets the grooves of the rough surface) (Berthier [19]). Both are stable equilibrium positions and offer local minimum energy states, but one may have lower energy than the other. A shift between the two states, i.e. wetting transition is possible if the droplet overcomes the energy barrier by internal or external means.

2.2. Diffusive evaporation

In the absence of convective flows over the droplet surface, the diffusion equation for evaporation is given by:

$$\frac{\partial c}{\partial t} = D \cdot \nabla^2 c \tag{3}$$

Evaporation can be considered as a quasi-steady-state process as the time required for the vapor concentration to adjust to changes of the droplet shape and surface temperature is on the order of $(r_b)^2/D_{AB}$ (Hu and Larson [9]), which is usually three orders of magnitude smaller than the total evaporation time of the micro-liter sized drops. The diffusion coefficient of vapor in the surrounding gas $D = 2.32 \times 10^{-5}$ m^2/s, McHale et al. [21].

The general diffusion rate equation for a sphere kept in an infinite medium, by assuming that the vapor concentration at the wet surface of the sphere, c_s is equal to its equilibrium concentration, is given by [22]:

$$\frac{dm}{dt} = 4\pi \cdot R_s \cdot D(c_s - c_\infty) \tag{4}$$

where c_∞ is the concentration of the vapor at infinite distance from the drop. The boundary conditions are, $c = c_s$ when $r = R_s$ and $c = c_\infty$ when $r = \infty$. An analogy between electric potential and diffusive flux can be invoked to calculate the rate of evaporation in case of a body of any shape [8]:

$$\frac{dm}{dt} = 4\pi \cdot D \cdot C_x(c_s - c_\infty) \tag{5}$$

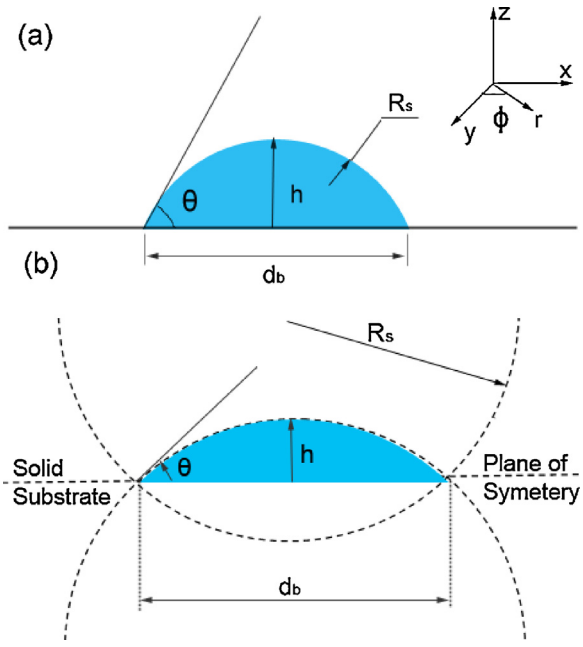

Fig. 1. (a) Profile of a droplet on a surface depicting the details of the coordinate system (b) shows two intersecting spheres forming an equi-convex lens [17].

where C_x is $C/4\pi\varepsilon_0$, C being the capacitance of the droplet and ε_0 is the permittivity of free space.

The evaporation of a sessile drop can thus be evaluated by half the capacitance of an isolated equiconvex lens of the same size and shape as the drop, as shown in Fig. 1. The approximated series solution that relates apex angle of the lens to relate the capacitance in the form of C/R_s was obtained from Picknett and Bexon [8]. The rate of evaporation of a sessile droplet with pinned contact line can be evaluated by:

$$\frac{dm}{dt} = -\frac{kEm_o^{2/3}(C/R_s)\sin\theta_o}{2\rho^{2/3}\sin\theta(t)} \tag{6}$$

where m_o is the initial mass of the droplet, and

$$k = 4\pi \cdot D \cdot (c_s - c_\infty) \tag{7}$$

$$E^3 = \frac{3}{\pi(1-\cos\theta(t))^2(2+\cos\theta(t))} \tag{8}$$

3. Experimental details

The effect of nano-porosity on wetting and bulk rate of evaporation of a droplet on a physically textured of an alumina surface has been investigated. Benchmarking of data for standard plain surfaces has been done before proceeding with nanoporous surfaces.

3.1. Details of set-up and sample surfaces

The details of different experimental set-ups used in this study for investigating wettability, spreading and evaporation is given below:

3.1.1. Spreading dynamics

For studying the droplet spreading dynamics, the sample is kept on a movable platform and the droplet is carefully placed on the sample using a needle (dia. = 200 μm), a syringe pump controlling the droplet volume. High speed photography captures spreading dynamics (resolution 1024 × 1024 at 2000 fps; Fastcam-Photron® SA-3). A Laser 3-D Confocal Microscope (Leica® HCA) is used to

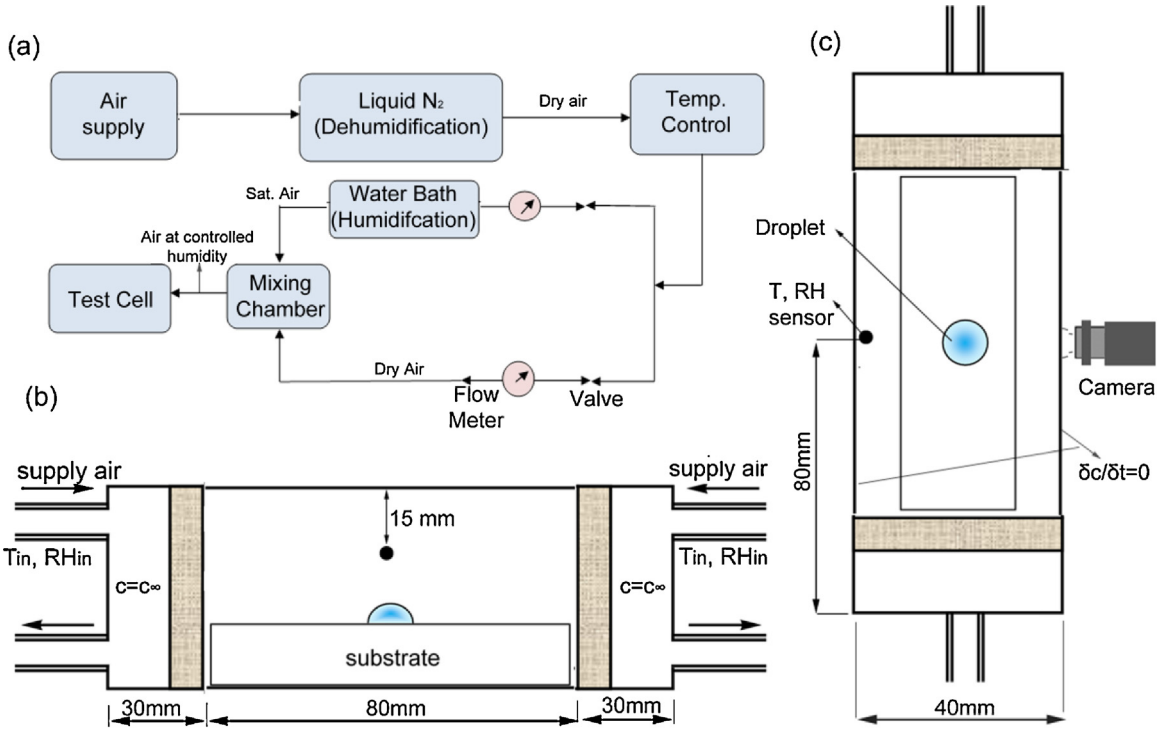

Fig. 2. (a) Basic sketch of the experimental set-up, (b) side view of the test cell with dimensions (c) top view of the test cell with position of camera [17].

generate slices (3D image stacks) of drops, doped with Rhodamine 6G fluorescent dye (Sigma–Aldrich®) after they reach equilibrium.

3.1.2. Evaporation of sessile droplets

The schematic of the experimental setup for controlled droplet evaporation explains the basic working principle, Fig. 2(a). The test cell (Fig. 2(b) and (c)) consists of a cubical chamber (8 cm × 4 cm × 4 cm), which is sufficiently large as compared to the size of the droplet, hence, satisfying the conditions at $r = \infty$. Two sides are exposed to constant humidity levels throughout the experiment, via a thick porous layer of paper (Dirichlet concentration boundary); the remaining four sides are insulated. Arrangement ensures that there is no bulk convection inside the test cell; evaporative transport is purely diffusive. The chamber is fitted with a combined temperature and humidity sensor (GE-ChipCap®). An isolated liquid droplet is placed at the center of the control volume using a micro-syringe and temporal variation of contact angle is captured by digital videography. For all experiments, deionized, degassed and filtered water is used. Glass and Teflon substrates are cleansed with mild bleaching solution and then treated with 5% ethanol solution in ultrasonic bath for 10 min to remove surface impurities.

3.2. Preparation of anodized nanoporous alumina (ANA) surfaces

To investigate the effect of nano-porosity on wettability and bulk diffusion evaporation rate, nanoporous alumina surfaces textured under controlled conditions are prepared. The following three morphologies of pores have been manufactured: (i) linearly aligned nanopores, (ii) randomly ordered nanopores, and (iii) organized hexagonal nanopores.

Anodized nanoporous alumina (ANA) was prepared using pure aluminum foil (99.9% Loba Chemie® and 99.999% Sigma–Aldrich®) of 100–125 μm thickness, which have micro- and nano-scratches as well and are anisotropically stressed along the rolling direction. Anodization of the cleaned aluminum (with acetone followed by sonication for 10 min) with 99.9% purity foil was carried out in a solution of oxalic acid (0.3 molar) at 40 V for 12 h at 18 °C for obtaining the ANA with linearly organized pores in the rolling direction. For obtaining ANA with other two morphologies, the aluminum foils of both purity levels are first electro-polished in an electrolyte made (mixture of ethanol and perchloric acid, 5:1, v/v) for ~5 min, which removes most of the surface scratches and stresses. For obtaining the ANA with pores organized in a random manner, a first anodization of the electro-polished aluminum foil of 99.9% purity in oxalic acid (0.3 molar) at 40 V and 18 °C for 12 h is sufficient. For the ANA with hexagonally organized pores, the electro-polished aluminum foil of purity 99.999% is first anodized at 0 °C, rest of the parameters being same. The formed alumina is etched off in a mixture of phosphoric acid, chromic acid and water (3.5 ml H_3PO_4, 4.5 g CrO_3/200 ml aqueous solution) at 90 °C for ~45 min. A second anodization for 12 h, keeping the rest of the parameters identical, resulted in highly organized nanopores in a hexagonal lattice. The pore size was controlled by etching in a solution of 5% phosphoric acid. We used samples with two kinds of pore sizes – small ones with an average pore size of (70 nm) and larger pores of average pore size (120 nm). The average pore spacing in all the samples used is 120 nm, the pore lengths being 29.76 μm (see Fig. 3). The average pore density is of the order 10^{15} pores/m^2.

3.3. Experimental procedure and data reduction

Firstly, the spreading and subsequent attainment of equilibrium of small micro-sized droplets is captured followed by digital image processing, providing the necessary information on apparent contact angle, radii, and height of the droplet. After attaining equilibrium, Laser fluorescence Confocal Microscopy provides the information in the third direction, used for reconstructing the entire three dimensional droplet shape.

Subsequently, evaporation of a 5 μl sessile droplet of water on plain and nanoporous surfaces is undertaken. The apparent contact

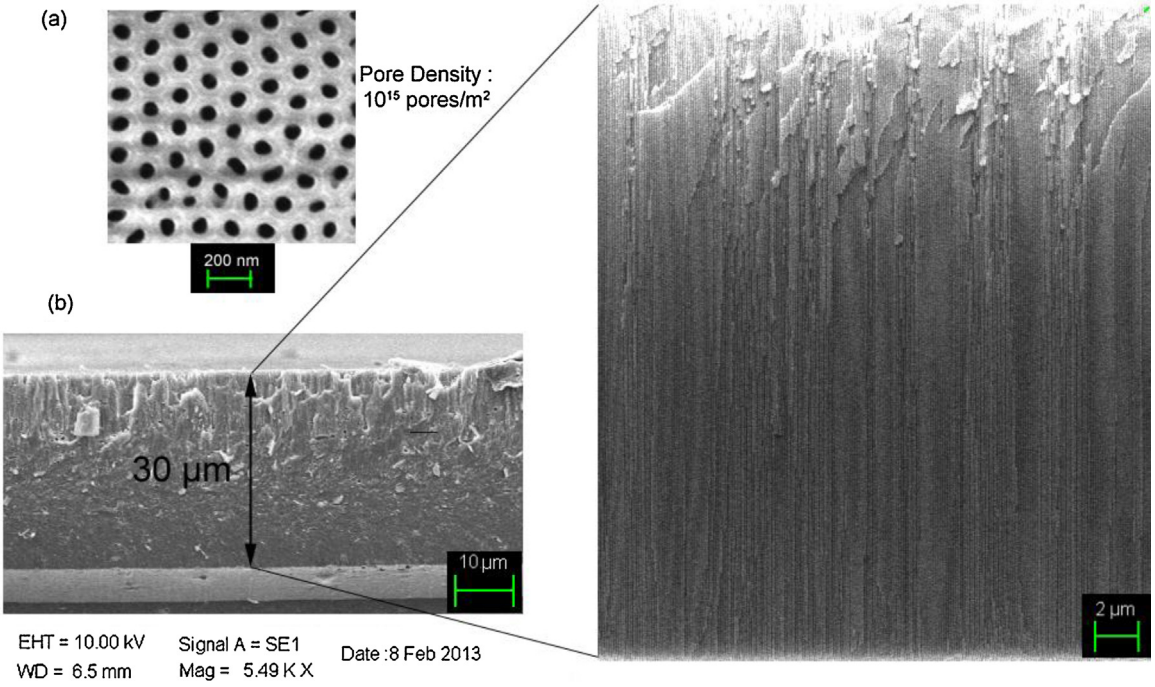

Fig. 3. SEM images (FESEM: Zeiss® Supra 40VP) showing (a) the top surface and (b) length of pores.

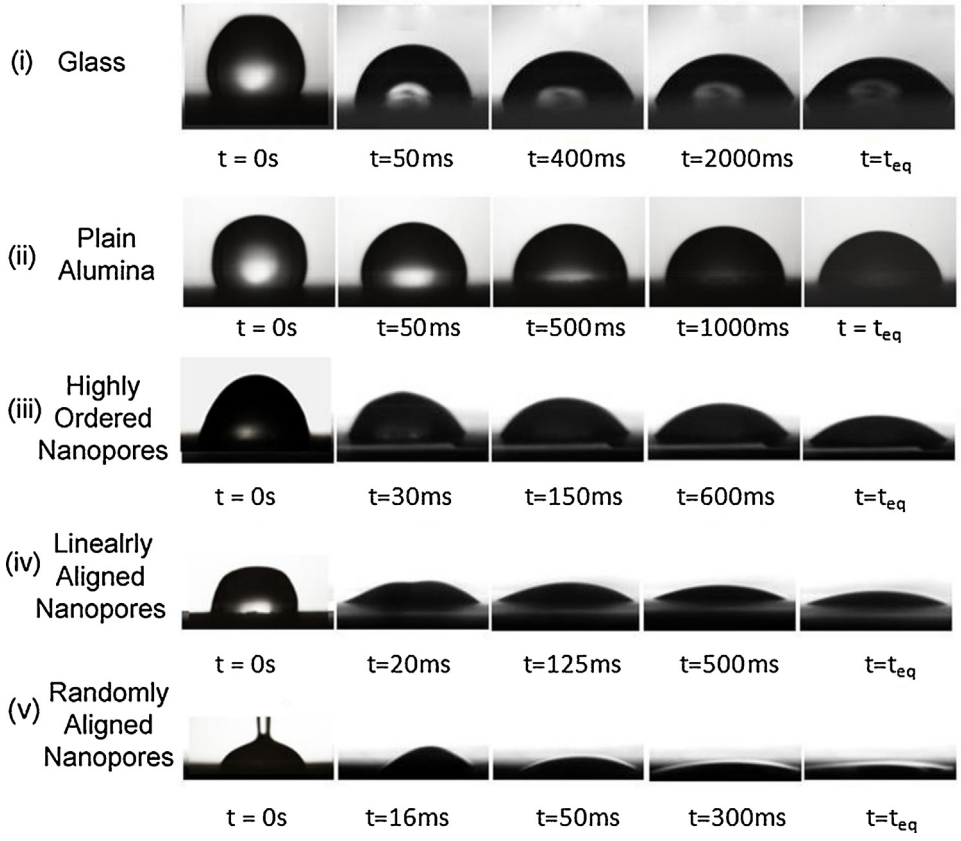

Fig. 4. Spreading dynamics of a 5 µl droplet on different surfaces (i–v), taken at 2000 fps using a high speed camera (magnification factor is different for different images to accommodate the final sizes).

angle of the droplet is monitored throughout the course of evaporation. Also, the rate of evaporation of a sessile droplet of ethanol on glass is studied for benchmarking with the existing model based on Eq. (6) [8]. For the purpose of measuring the equilibrium contact angle, tool using DropSnake algorithm in ImageJ® software, which is based on B-spline snakes (active contours), is used. The results thus obtained are compared and reported in the next section.

4. Results and discussion

4.1. Spreading of droplets on surfaces

Fig. 4(i)–(v) shows the spreading dynamics of a 5 μl water droplet on a borosilicate glass substrate, plain alumina surface, ANA with organized, linearly aligned and randomly distributed nanopores, respectively. The final equilibrium contact angle obtained is 44.6° for glass, 62.2° for plain alumina, 12.1° for ANA with organized nanopores and ~8.9° for linearly aligned nanopores. The droplet completely spreads on surface with randomly distributed pores, losing its identity completely. Thus, the nanoporous structure drastically affects wettability of the substrate.

According to Bonn et al. [1], when drop radius (r), $r < l_c$ (as well as small volume $V^{1/3} < l_c$), the Tanner's law given by Eq. (1) can be applied to the spreading droplet. The final contact radius of the droplet in this study is $r_b = 1.4$ mm and $V^{1/3} = 1.71$ mm which is less than the capillary length $l_c = 1.9$ mm for water. The initial part of Fig. 5(a) and (b) show some deviation from linear behavior owing to the disturbance that arises from the residual kinetic energy of the droplet coming from needle injection. The value of constant α for Tanner's law is $\alpha = 0.809$ mm/s$^{1/10}$. Tanner's law gives value of $\alpha = (1.09/B)^{1/10}$ mm/s$^{1/10}$, which gives the value of constant $B^{1/10} = 1.25$ for water on glass. For the water on plain alumina surface, the value of constant $\alpha = 0.758$ mm/s$^{1/10}$; which gives the value of $B^{1/10} = 1.33$ which is close to theoretical estimate of its value ~1.2 given by Bonn et al. [1]. During the execution of the experiment, the droplet radius was non-zero. In addition, in spite of the best efforts, there is a finite 'free fall' through which the gravity force affects the initial condition, just when the drop touches the substrate. The intercept on the Y-axis is a result of this error, wherein at $t = 0$, r_o is finite. From the videographic images, the correction comes out to be approximately 0.611 mm while the outcome of the scaling, provided by the best fit curve is 0.552 mm.

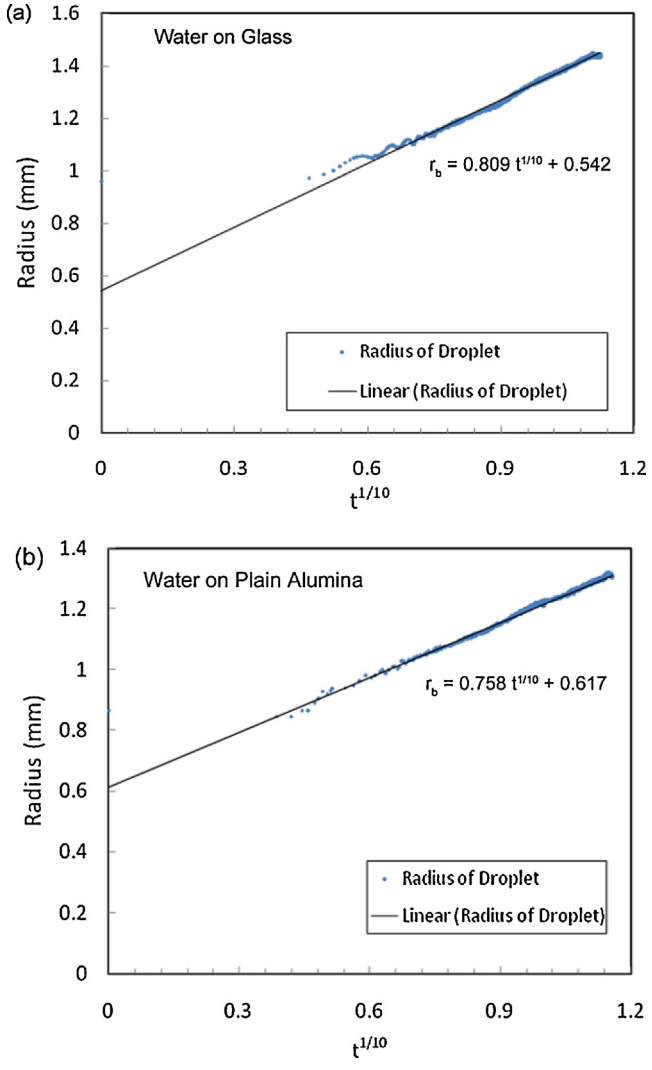

Fig. 5. Plot of base radius of a 5 μl droplet on (a) glass and (b) plain alumina respectively, vs. tenth power of time to benchmark the set-up with Tanner's law.

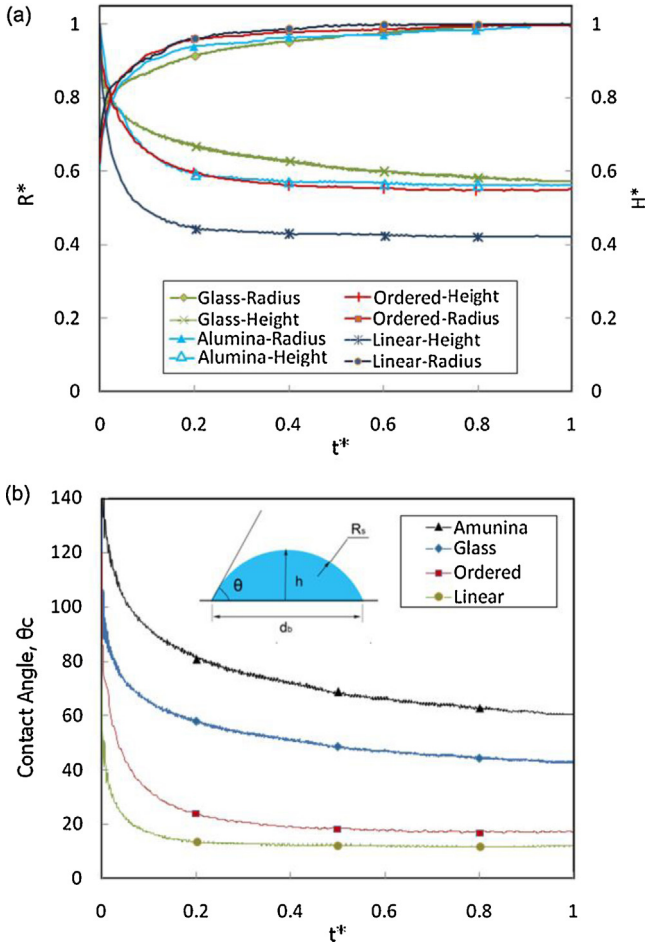

Fig. 6. (a) Plot of non-dimensional radius and height with time as a 5 μl droplet spreads on surfaces with different morphologies. The definitions of the different terms are given in Table 1; (b) variation of contact angle with time.

Fig. 6(a) shows the variation of non-dimensional radius R^* and non-dimensional height H^* vs. time for glass, plain alumina and different nanoporous surfaces. Table 1 shows the initial/equilibrium values of different parameters monitored. The plot of H^* vs. t^* starts from unity, as H_o is used as the normalizing factor and the plot of R^* vs. t^* begins from different value to finally converge at unity, as R_{eq} is taken as the normalizing factor. It is observed that the rate of spreading is higher on nano-porous surfaces as compare to both

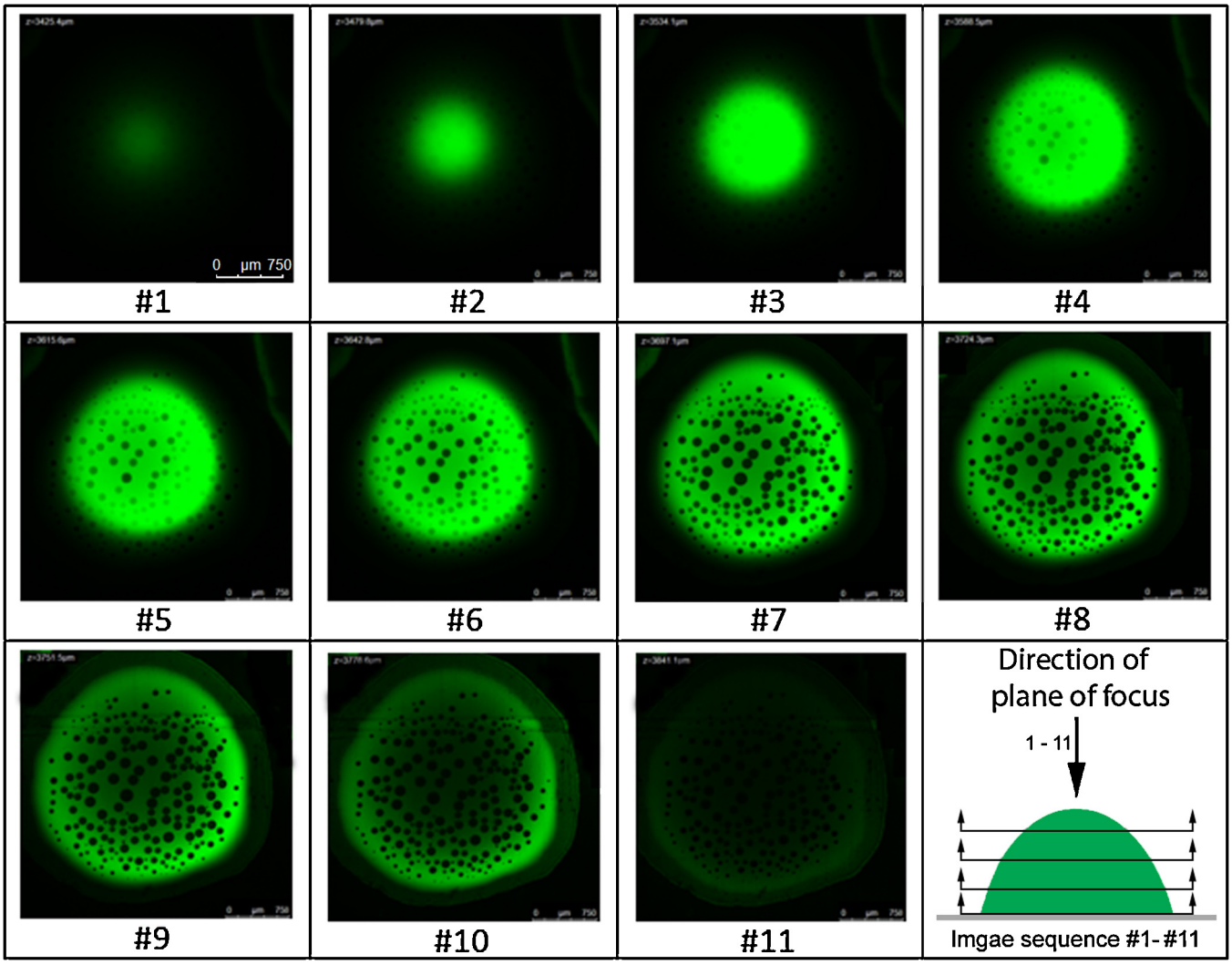

Fig. 7. The Z-sequence of images obtained from Laser confocal microscope showing different planes of a droplet in equilibrium on a nano-surface. Each step size is 28 µm.

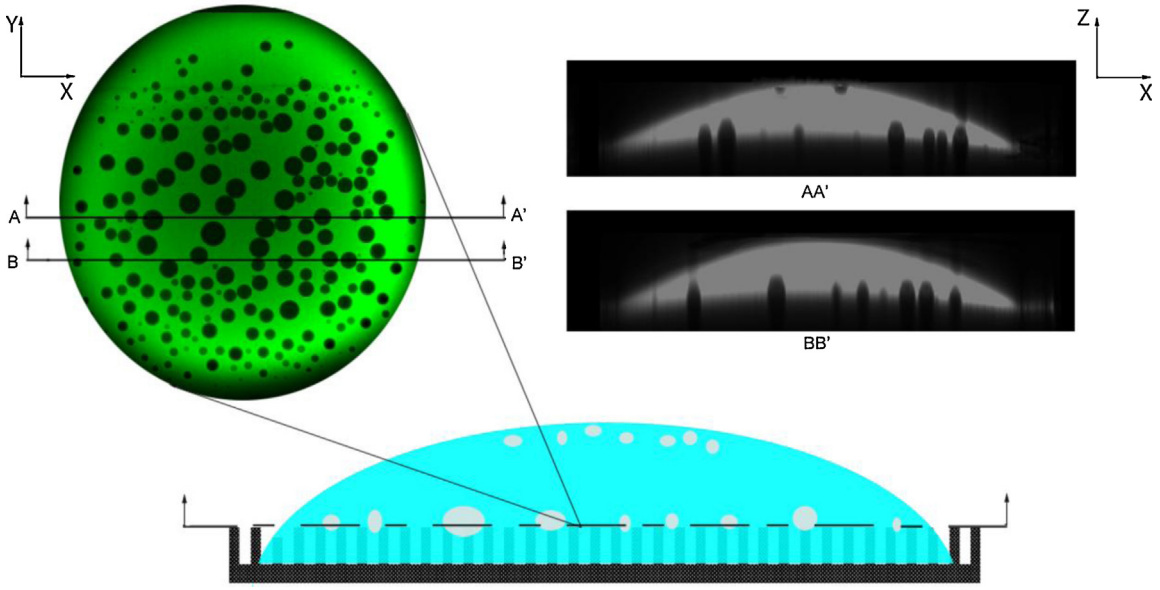

Fig. 8. Section of two planes of the droplet on a nano-surface. The air bubbles can be seen adhering to the surface as well as at the interface of the droplet in equilibrium on these textured surfaces.

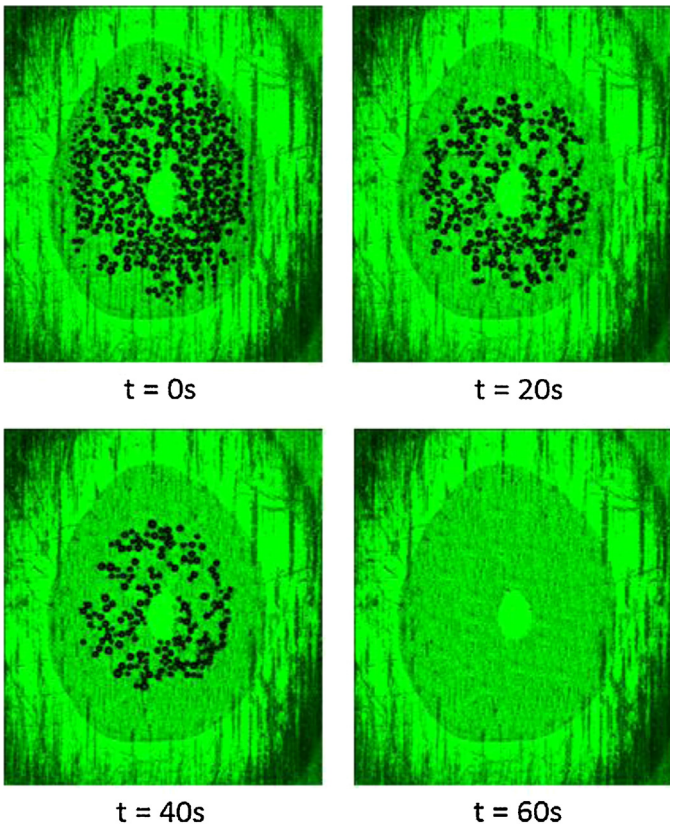

Fig. 9. Confocal image of a plane of droplet in equilibrium on a surface randomly ordered nano-pores to show escaping bubbles.

glass and plain alumina. Also, it is seen that the rate of spreading is very high initially and becomes sluggish toward the end. The increased rate and extent of spreading on nanoporous surface could be attributed to the formation of small capillaries between nano-pores which facilitates the flow of water. Also, random alignment of these capillaries gives more freedom to water to spread on the surface.

The variation of contact angle with time as the droplet is spreading on the substrate is shown in Fig. 6(b). The rate of change of contact angle is higher in the initial phase of spreading and decreases slowly, the effect being more pronounced for nano-porous surfaces. The final contact angle is lowest for surface with random aligned nano-pores where the droplet fully spreads (water enters the pores while the rest of it forms a thin film over the surface); for which the data is not shown because the height of the droplet is very less and cannot be processed accurately.

4.2. Laser Confocal Microscopy of equilibrium drops

It is observed that when a water droplet is put on a nano-structured surface, it initially adopts the Cassie state. However, the transition to the Wenzel state is quick and the air entrapped in nano-pores starts oozing out within a fraction of second. The small bubbles thus formed merge with other adjoining ones to from bigger bubbles which are then visible to the naked eye. In sessile mode, due to gravitational force, some of the bubbles leave the surface too and move toward the interface.

Fig. 7 shows Z-sequence of images obtained from confocal microscope which provides an evidence of wetting state transition from Cassie to Wenzel. The droplet cannot adopt Wenzel state as soon as it is put on these surfaces as there is no room for air entrapped in pores to escape. As the air escapes with time from these pores, a higher density of air bubbles adhering to the substrate is observed.

Fig. 8 shows X–Z plane reconstructed from Z-sequence of images obtained from con-focal microscope. The bubbles emerging out of nano-pores on the surfaces as well as interface can be clearly seen in this plane. Fig. 9 shows bubbles escaping from the interface in due course of evaporation. As contact line moves inwards, the bubbles which are present at the edge of the droplet escape first. Also, some of the larger bubbles escape from interface of the droplet as they grow bigger due to coalescence.

Table 1
Value of t_{eq} – time taken by droplet to achieve equilibrium; D_{eq} – equilibrium diameter; H_o – Initial height of droplet on different morphologies of nano-porous surfaces.

Surface	t_{eq} (s)	D_{eq} (mm)	H_{ini} (mm)
Glass	3.226	2.88	1.61
Plain alumina	2.034	2.04	1.75
Ordered nanopores	0.56	3.51	1.50
Linearly aligned nanopores	0.984	2.91	1.93

Here, $H^* = H/H_o$, $R^* = R/R_{eq}$ and $t^* = t/t_{eq}$.

4.3. Diffusive evaporation of sessile droplets

Fig. 10(a) presents comparison results obtained from analytical model given by Picknett and Bexon [8] and the results obtained from experiments on glass and Teflon. It can be observed that the results agree quite well with the model with minor discrepancy. This can be attributed to the fact that while the theory is for diffusion in infinite medium, the experimental test cell although large, is still of finite size. The model works well for other simple fluids like ethanol evaporating on glass as well (details not reported here for brevity). Experimentally it is observed that an ethanol droplet of 5 μl with an initial contact angle of 21.2° takes about 420 s to completely evaporate. The results obtained from the models gives an evaporation time of about 395.2 s which comes to be within an error band of about 5.7%.

The observed initial contact angle of a water droplet on glass (44.6°) and Teflon (94.2°) is irrespective of the change in RH of the vicinity as seen in Fig. 10(b). The variation of contact angle with time at various humidity levels is also shown in the figure. It is observed that the variation of contact angle is nonlinear and this nonlinearity increases as the RH increases. Another interesting phenomenon to be observed (see Fig. 11) is that the contact line remains pinned for major part of the time and de-pinning occurs only after the contact angle becomes less than about 8°.

It is observed that the rise in humidity level is detected by the sensor soon as the droplet is placed on the surface. The RH at the sensor location keeps rising for the initial few minutes due to diffusion flux; becomes stable for some time and then, starts gradually falling back to base level toward the end. The recorded RH inside the chamber takes about 1 min to fall back to base level after the drop has visually disappeared. However, no significant change in temperature is observed throughout the process.

For all nano-structured surfaces, the droplet almost completely spreads on the substrate, making an apparent contact angle approximately equal to 10° or lower, depending on the pore morphology and/or the state of wetting transitions. Accurate quantitative measurement of this contact angle is not-trivial and was not attempted in this work. The theory of Picknett and Bexon [8] requires the volume and the radius/apparent contact angle of the droplet on the substrate for prediction of the rate of evaporation. Thus, to apply this theory on nanoporous substrates, the apparent contact angle of the droplet (which spreads as a thin film) can only be assumed. For comparative purpose, Fig. 12(a) includes the results obtained by this theory for arbitrarily assumed apparent contact angles of 10°, 5° and 2°. As can be seen, while the theory is qualitatively

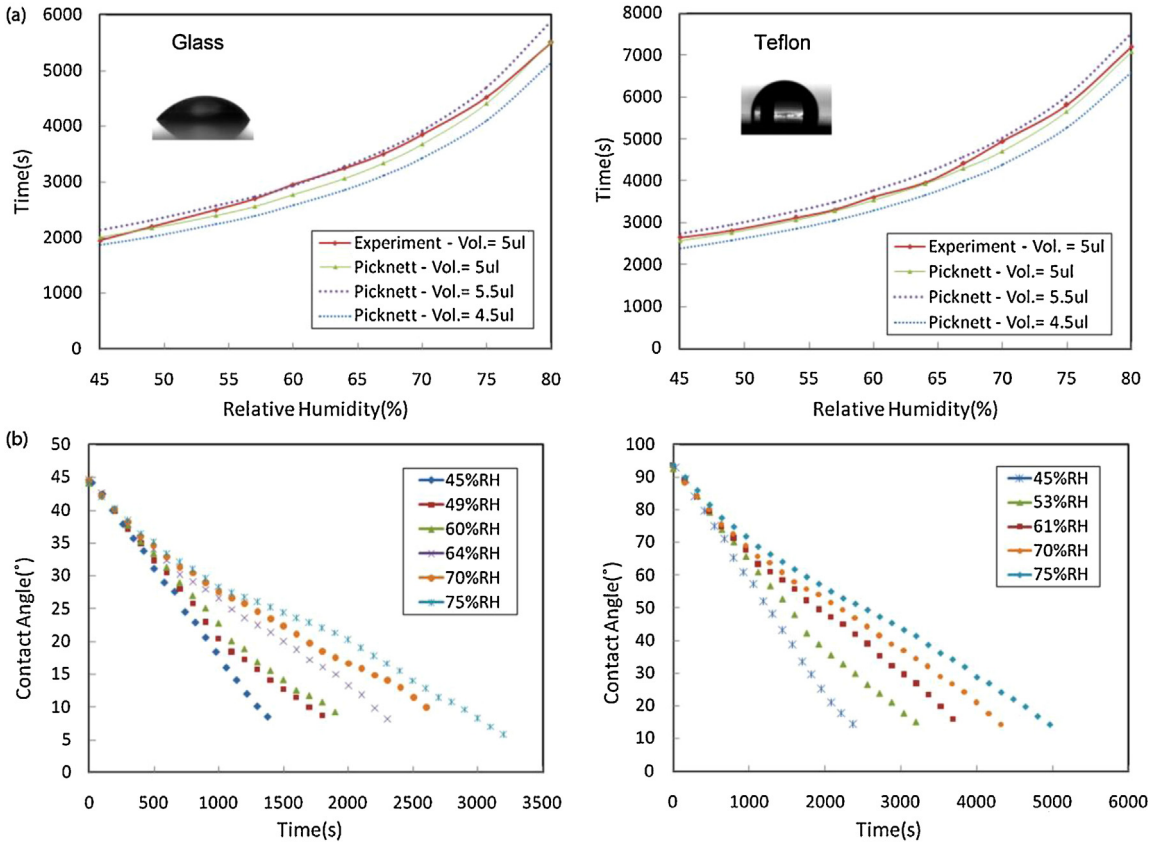

Fig. 10. (a) Time taken by 5 μl water droplet to evaporate on a glass on the left and Teflon on the right at different relative humidity. The results from theoretical model is also present for 4.5, 5, 5.5 μl droplets. In inset (i) 5 μl droplet of water on glass with a contact angle of 44.6°, (ii) 5 μl droplet of water on Teflon with a contact angle of 94.2°; (b) contact angle variation of an evaporating 5 μl water and Teflon droplet after different humidity levels.

quite satisfactory for the nano-porous substrates, quantitative prediction is subject to accurate measurement of the apparent contact angle of the droplet on these nano-porous substrates.

It is observed that the spreading and wettability increase as the orderliness of pore distribution decreases, which eventually leads to a high rate of evaporation (Fig. 12(a)). As explained in the previous section, the emergence and movement of air and bubbles is expected to disturb the local hydrodynamics (Marangoni convection) inside the droplet which eventually alters the rate of evaporation on these surfaces. Also, due to greater amount of spreading on the nanoporous surfaces, the final contact area is more; which gives more area for vapor flux to diffuse from the droplet. On the surfaces with larger nanopores irrespective of distribution morphology, the volume of gas expelled out of the pore is more and it is proposed that this increased density of bubbles tends to agitate the bulk fluid due to micro-convection induced by movement of bubbles inside the droplet, thus improving the rate of evaporation. This aspect needs further scrutiny. Also, SEM images of different nanoporous surfaces are shown in Fig. 12(b).

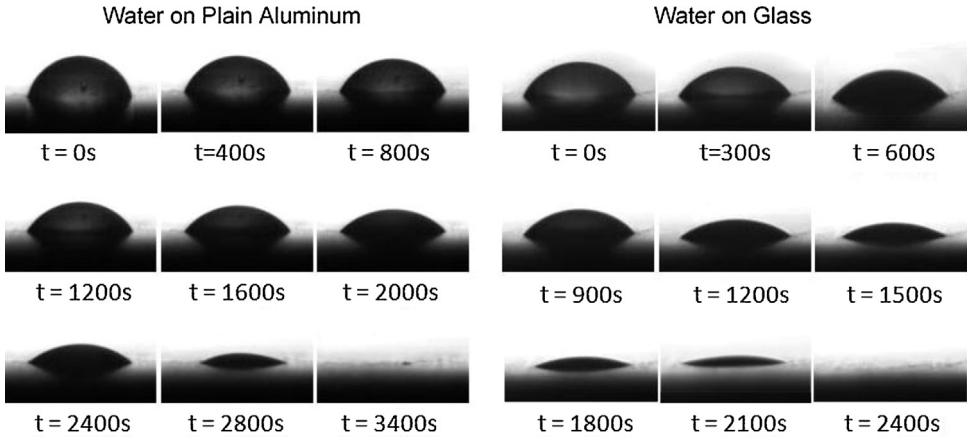

Fig. 11. Images of droplet evaporating with contact line pinned on a plain alumina surface and glass at 45% RH.

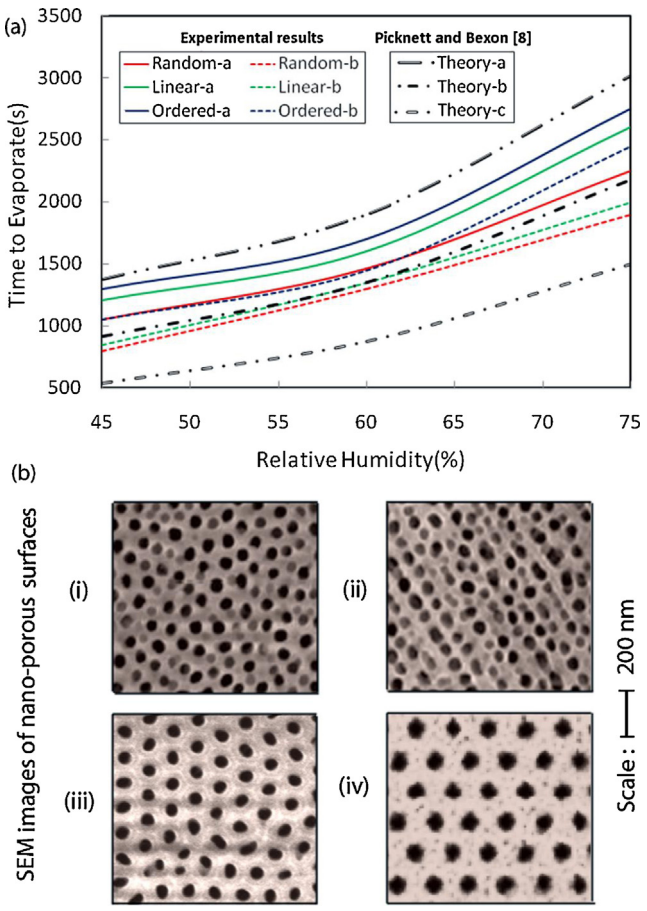

Fig. 12. (a) Time taken to evaporate a 5 μl water droplet on the three nanoporous alumina surfaces. The dotted lines for each case show the results from larger pore size. The theoretical result [8] on nano-porous substrate has been obtained by assuming an apparent contact angle of 10°, 5° and 2°, represented by theory – a, b and c respectively; (b) – (i)–(iii) SEM images of surfaces with randomly, linearly ordered and organized nanopores and (iv) surface with ordered pores, after pore widening.

The rate of evaporation tends to be highest on the surface with randomly oriented pores followed by surface with linearly aligned pores and surface with organized hexagonally pores. Also, the similarity in results on wettability in Section 4.1 and rate of evaporation is consistent with the previous studies [7] who reported that the rate of evaporation of small spherical sector drops is proportional to the vapor–air contact area (i.e. square of radii). This relates the extent of spreading with bulk evaporation rate as more spreading leads to a greater final contact radius.

5. Summary and conclusions

In this study we investigated the spreading dynamics and evaporation of a droplet on plain and nanoporous surfaces in a controlled environment. The results obtain clearly depict that nano-structuring can effectively alter the wettability of an alumina surface. The presence of nanopores increases the wettability of water on alumina and the droplet fully wets some of the samples, losing its identity completely. The pattern of distribution of nano-pores affects equilibrium contact angle of a droplet. This, in fact, could have a direct influence on heat transfer coefficient which needs further exploration. Also, a wetting state transition from Cassie to Wenzel, confirmed by results from Laser Confocal Imaging, is observed on these surfaces, which reduces the final static equilibrium contact angle drastically.

It can be inferred from the results on plain and textured surfaces as well as the theory that the time taken to evaporate and contact angle of the droplet does not change linearly with increase in relative humidity. The size and distribution morphologies of nanopores can significantly affect the evaporation dynamics of a droplet. The bulk rate of evaporation is significantly altered as randomness in the distribution of these pores increases. Also, increasing the nanopore size has a similar effect.

Future work on this may include the coupling of energy equation with diffusive process as there can be sizable change in temperature of the droplet as it evaporates. As suggested by some recent studies, the thermal properties of the substrate may also affect the evaporation process, making the heat transfer conjugate in nature. Also, the study can be extended to evaporation of colloidal fluids with nano-particles and their interaction with nano-structured surfaces.

Acknowledgements

SK would like to acknowledge the fellowship program of the German Academic Exchange Service (DAAD), which facilitated his interaction on this topic of research with Prof. Peter Stephan at TU-Darmstadt, Germany. The contribution of Mr. M. Siddhardh Chandra (M.Sc.) in design and fabrication of the experimental setup and its benchmarking is also acknowledged. Confocal Microscopy facility has been funded by the Department of Science and Technology, Government of India, under the FIST scheme.

References

[1] D. Bonn, J. Eggers, J. Indekeu, J. Meunier, E. Rolley, Wetting and spreading, Rev. Mod. Phys. 81 (2) (2009) 739–804.
[2] H.Y. Erbil, Evaporation of pure liquid sessile and spherical suspended drops: a review, Adv. Colloid Interface 170 (2012) 67–86.
[3] T. Sun, L. Feng, X. Gao, L. Jiang, Bioinspired surfaces with special wettability, Acc. Chem. Res. 38 (2005) 644–652.
[4] M.A.C. Stuart, W.T.S. Huck, J. Genzer, M. Müller, C. Ober, M. Stamm, G.B. Sukhorukov, I. Szleifer, V.V. Tsukruk, M. Urban, F. Winnik, S. Zauscher, I. Luzinov, S. Minko, Emerging applications of stimuli-responsive polymer materials, Nat. Mater. 9 (2) (2010) 101–113.
[5] P. Tabeling, Microfluidics, EDP Sciences, Paris, 2004, ISBN 978-0-1985-6864-3.
[6] V. Deprédurand, G. Castanet, F. Lemoine, Evaporative heat transfer characteristics of a water spray on micro-structured silicon surfaces, Int. J. Heat Mass Transfer 53 (2010) 3495–3502.
[7] S.M. Rowan, M.I. Newton, G. McHale, Evaporation of microdroplets and the wetting of solid surfaces, J. Phys. Chem. 99 (1995) 13268–13271.
[8] R.G. Picknett, R. Bexon, The evaporation of sessile or pendant drops in still air, J. Colloid Interface Sci. 61 (2) (1977) 336–350.
[9] H. Hu, R.G. Larson, Evaporation of a sessile droplet on a substrate, J. Phys. Chem. B 106 (2002) 1334–1344.
[10] R. Bhardwaj, An investigation of the evaporation of a droplet on a solid surface: evaporation, self-assembly of colloidal deposits, and interfacial heat transfer, Columbia University, 2010 (Ph.D. thesis).
[11] R.D. Deegan, O. Bakajin, T.F. Dupont, G. Huber, S.R. Nagel, T.A. Witten, Capillary flow as the cause of ring stains from dried liquid drops, Nature 389 (1997) 827–829.
[12] R.H. Chen, T.X. Phuoc, D. Martello, Effects of nanoparticles on nanofluid droplet evaporation, Int. J. Heat Mass Transfer 53 (2010) 3677–3682.
[13] C.Y. Lee, B.J. Zhang, J. Park, K.J. Kim, Water droplet evaporation on Cu based hydrophobic surfaces with nano and micro-structures, Int. J. Heat Mass Transfer 55 (2012) 2151–2159.
[14] C.H. Choi, C.J. Kim, Droplet evaporation of pure water and protein solution on nanostructured superhydrophobic surfaces of varying heights, Langmuir 25 (13) (2009) 7561–7567.
[15] B. Sobac, D. Brutin, Triple-line behavior and wettability controlled by nanocoated substrates: influence on sessile drop evaporation, Langmuir 27 (2011) 14999–15007.
[16] B. Sobac, D. Brutin, Thermal effects of the substrate on water droplet evaporation, Phys. Rev. E 86 (2012) 0216021–216110.
[17] S.K. Singh, D. Pratap, S.A. Ramakrishna, S. Khandekar, Evaporation of sessile droplets on nano-porous alumina surfaces, in: Proc. Int. Symp. on Multi-Phase Flow, Heat-Mass Transfer and Energy Conversion, Paper No. FG-45, Xian, China, 2012.
[18] C. Ran, G. Ding, W. Lui, Y. Deng, W. Hou, Wetting on nanoporous alumina surface: transition between Wenzel and Cassie states controlled by surface structure, Langmuir 24 (2008) 9952–9955.

[19] J. Berthier, Microdrops and Digital Microfluidics, 2008, ISBN 978-0-8155-1544-9.
[20] L.H. Tanner, The spreading of silicone oil drops on horizontal surfaces, J. Phys. D 12 (1979) 1473–1484.
[21] G. McHale, S.M. Rowan, M.I. Newton, M.K. Banerjee, Evaporation and the wetting of a low-energy solid surface, J. Phys. Chem. B 102 (1998) 1964–1967.
[22] J.C. Maxwell, Diffusion Collected Scientific Papers, vol. 2, Cambridge, 1890, pp. 625–650.